Noise reduction in LOS wind velocity of Doppler lidar using discrete wavelet analysis

Songhua Wu (吴松华), Zhishen Liu (刘智深), and Dapeng Sun (孙大鹏)

Ocean Remote Sensing Laboratory of the Ministry of Education of China, Ocean Remote Sensing Institute (ORSI), Ocean University of China, Qingdao 266003

Received July 7, 2003

The line of sight (LOS) wind velocity can be determined from the incoherent Doppler lidar backscattering signals. Noise and interference in the measurement greatly degrade the inversion accuracy. In this paper, we apply the discrete wavelet denoising method by using biorthogonal wavelets and adopt a distance-dependent thresholds algorithm to improve the accuracy of wind velocity measurement by incoherent Doppler lidar. The noisy simulation data are processed and compared with the true LOS wind velocity. The results are compared by the evaluation of both the standard deviation and correlation coefficient. The results suggest that wavelet denoising with distance-dependent thresholds can considerably reduce the noise and interfering turbulence for wind lidar measurement.

OCIS codes: 280.3640, 280.3340, 100.7410.

The line of sight (LOS) wind velocity can be retrieved from the incoherent Doppler lidar backscattering signals[1−6]. The Doppler lidar is an active remote sensing instrument that emits laser pulses towards the atmosphere and measures the Doppler shift of the collected return signal. The frequency shift results from the relative movement of the scatter elements along the LOS of lidar, which relates to the mean wind in the observed volume. Laser is scattered either by aerosol particles (Mie scattering) or by air molecules (Rayleigh scattering). Lidar backscatters contain a variety of noise and interferences. LOS wind velocity errors become extremely high when the noise in lidar returns contributes a significant amount to the wind ratio fluctuations. Attenuating this kind of noise is essential for the precise wind measurement and subsequent data analysis.

The Fourier smoothing technique has long been used for reducing noise. Taking low-pass (LP) filter as an example, one usually sets a cutoff frequency to remove noise that all the frequency components above the cutoff are zero. LP filter can smooth the noisy components but blur the edges of the reconstructed signal. Contrastively, the edges get sharper but the noisy components are amplified when using the high-pass (HP) filter. Actually, the Gaussian white noise contributes to all frequencies equally. In Fourier smoothing filtering, a common assumption is that the information content of a signal can be separated from the noise by taking into account that the signal varies slowly in comparison to the noise. Since LOS velocity signals represent spatially varying frequency components, setting a particular cutoff frequency may result in signal distortion by removing some necessary signal components. Contrastively, wavelet denoising technique shrinks wavelet coefficients to zero. Usually a few wavelet coefficients preserve almost the whole energy of the signal. As a result, the wavelet shrinkage removes the noise without distorting the signal.

In this work, the LOS velocity data obtained from measurements and simulation program are analysed by discrete wavelet transform. We used biorthogonal wavelets as the prototype wavelets and adopted a distance-dependent threshold algorithm on the denoising procedure. Experimental data were gathered from *in situ* data and lidar simulation software. The lidar simulation program is based on the direct detection method where the backscattering signal is analysed by a frequency discriminator such as iodine filter and interferometer. The denoising results are evaluated by comparing both the standard deviation and correlation coefficient.

A virtual instrument system for the incoherent Doppler lidar simulation, similar to our real incoherent Doppler lidar, MIDWiL[5,6], was developed by Ocean Remote Sensing Institute, OUC[7]. It is "equipped" with a second harmonic Nd:YAG laser which emits 150-mJ light pulses of 8-ns duration upwards into the atmosphere. Backscattered photons are collected by a telescope with 0.3 m diameter. The photons go through two detection channels: one is the energy reference channel and the other is the frequency discriminator by using iodine filter and a Fabry-Perot interferometer.

We selected three groups of true and simulated wind profiles (W_1, W_2 and W_3) generated by this virtual system for wavelet analysis. The data covers a range from 11 km to 27 km where Rayleigh backscattering contributes the most to the total backscatters. The Rayleigh spectrum is Gaussian with its width given by the temperature of the atmosphere. We introduced the wind speed fluctuations according to related atmospheric parameters (calculated from model temperature, pressure and transport coefficients). Dark current and electron fluctuations are also taken into account in the simulation. The actual number of photon and electron fluctuations in detection channels is assumed to obey the Poisson distribution. The data set will consist of results both from Mie scattering and Rayleigh scattering after the combination of *in situ* data and data obtained by using the Mie scattering model. The data will be able to cover the region from the ground up to the stratosphere.

Wavelets process data are at different scales or resolutions[8]. In wavelet analysis, one adopts a wavelet prototype function called the analyzing or mother wavelet. Let $\psi(x)$ be the analyzing wavelet defined in the

space of square-integrable functions over the real numbers $L^2(R)$. An orthogonal basis is constructed through dilations and translations of $\psi(x)$

$$\psi_{a,b}(x) = \frac{1}{\sqrt{|a|}}\psi\left(\frac{x-b}{a}\right), \quad (1)$$

where $a \neq 0$, $b \in R$, a is a scale factor that gives dilations and compressions and b is a translation in time. The translation factor b represents the sliding of $\psi(x)$ over a given time series $F(t)$. The continuous wavelet transform of a time series $F(t) \in L^2(R)$ is defined as

$$\Phi_h f(a,b) = \frac{1}{\sqrt{c_h}} \cdot \frac{1}{\sqrt{|a|}} \cdot \int_{-\infty}^{+\infty} f(x)\overline{\psi}(\frac{x-b}{a})\mathrm{d}x, \quad (2)$$

$$c_h = 2\pi \int_{-\infty}^{+\infty} \frac{|\bar{h}(\omega)|}{\omega}\mathrm{d}\omega < \infty. \quad (3)$$

The reconstruction of $f(x)$ using $\Phi_h f(a,b)$

$$f(x) = \frac{1}{\sqrt{c_h}} \int_{R\times R} [\Phi f(a,b)]|a|^{-\frac{1}{2}} h\left(\frac{x-b}{a}\right)\frac{\mathrm{d}a\mathrm{d}b}{a^2}. \quad (4)$$

Since the theory and fast computing algorithm of discrete wavelet analysis have been widely discussed[8], we do not get into details in this paper. In this work we used the biorthogonal wavelets (Bior4.4) as the analyzing wavelets, which are biorthogonal, symmetry and regular wavelets with an explicit expression. We have evaluated several analyzing wavelets such as Daubechies and Dmeyer before this experiment. Daubechies and Dmeyer are as good as the biorthogonal wavelets for low to medium noise variances, but the biorthogonal wavelets work much better in the whole domain of noise variances to avoid signal distortion. The class of orthogonal wavelets is widely used in multiresolution analysis.

Biorthogonal wavelets present the property of the linear phase, which is necessary for signal reconstruction. It is known that symmetry and exact reconstruction are incompatible (excepting the Haar wavelet) if the same FIR filters are used for reconstruction and decomposition. By using two wavelets, one for decomposition and the other for reconstruction, biorthogonal wavelets are able to achieve symmetry and exact reconstruction[9].

$\overline{\psi}$ is the analysis wavelet, and the coefficients of the signal s are

$$\overline{c}_{j,k} = \int s(x)\overline{\psi}_{j,k}(x)\mathrm{d}x. \quad (5)$$

ψ is the synthesis wavelet

$$s = \sum_{j,k} \overline{c}_{j,k}\psi_{j,k}. \quad (6)$$

The wavelets $\overline{\psi}$ and ψ are related in the following way

$$\int \overline{\psi}_{j,k}(x)\psi_{j',k'}(x)\mathrm{d}x = 0 \text{ when } j \neq j' \text{ or } k \neq k', \quad (7)$$

$$\int \overline{\phi}_{0,k}(x)\phi_{0,k'}(x)\mathrm{d}x = 0 \text{ when } k \neq k'. \quad (8)$$

The general denoising procedure involves decomposition, thresholding and reconstruction. In this application, the simulated wind profile is first decomposed into the approximations and details using biorthogonal wavelets. The approximations are the high-scale, low-frequency components, while the details are the low-scale, high-frequency components. According to the principle of Stein's Unbiased Estimate of Risk (SURE), the thresholds are calculated for the detail coefficients of each level.

The SURE threshold selecting principle is

$$T = \sqrt{2\log_e[n\log_2(n)]}, \quad (9)$$

where n is the signal length.

In order to handle nonstationary noise, distance-dependent (time-dependent) thresholds are defined. Lidar backscatters have great dynamic magnitude over 10^5. Because of the small number of backscattered photons in the far distance, the LOS wind velocity is noisier at higher atmospheric regions. A simple scheme to attenuate noise is to compute thresholds and zero or downweight the coefficients below these thresholds[10]. However, it might result in signal distortion if the noise is not Gaussian but especially large amplitude. Actually, the noise can vary with laser transmission distance. Thus, we define the distance-dependent thresholds to improve the capability of handling nonstationary noise. Different threshold values are used at each distance interval. The intervals as well as the values are dependent on the noise level of the LOS signal. The practical results in this work are obtained with 2 or 3 intervals. Table 1 lists the thresholds for three groups of simulation data at each interval.

Next, we applied soft thresholding to downweight the noise coefficients. Finally, the signal is reconstructed by using the original approximation coefficient of level 4 and the modified detail coefficients from levels 1 to 4.

The soft thresholding strategy is applied due to its nice mathematical properties[10]. It first zeros the elements whose absolute values are lower than the threshold and then shrink the nonzero coefficients towards zero with no discontinuities at that point.

Figure 1 shows the performance of wavelet denoising for the LOS wind velocity profile. Three groups of profile are plotted, involving true data, simulation data and denoised simulation data. Filled circles represent the true wind velocity profile. The gray vertical lines are the simulation wind velocity profiles created by simulation software. The diamonds are denoised simulation wind velocity profiles obtained by using wavelet analysis.

Figure 2 shows the linear regression through origin for the simulation LOS wind velocity data and wavelet denoised data as the function of true wind. We can see considerable improvements of the standard deviation (SD) and correlation coefficient (R) from the comparison between (a) and (b), (c) and (d), (e) and (f) in Fig. 2. The SD of the first figure among three groups of data (6.15, 3.22 and 2.62 m/s respectively) is big primarily due to the noise caused by the variation of atmospheric parameters, dark current and electron fluctuations. Correspondingly, the SD of the denoised data with the turbulence and noise being significantly reduced by wavelet denoising is 1.55, 1.08 and 0.97 m/s, respectively.

Table 1. Thresholds List

Wind Profile	Distance-Dependent Threshold Interval	Decomposition Level 1	2	3	4	5
W_1	Interval 1	3.417	6.313	1.770	1.393	—
	Interval 2	13.280	23.140	5.309	1.714	—
	Interval 3	17.080	27.860	11.370	2.520	—
W_2	Interval 1	2.384	1.218	1.150	2.227	—
	Interval 2	12.600	5.154	6.190	1.655	—
W_3	Interval 1	1.741	0.603	0.900	0.552	0.278
	Interval 2	7.876	11.040	5.648	5.914	5.674
	Single Threshold	0.397	2.397	0.740	1.651	1.117

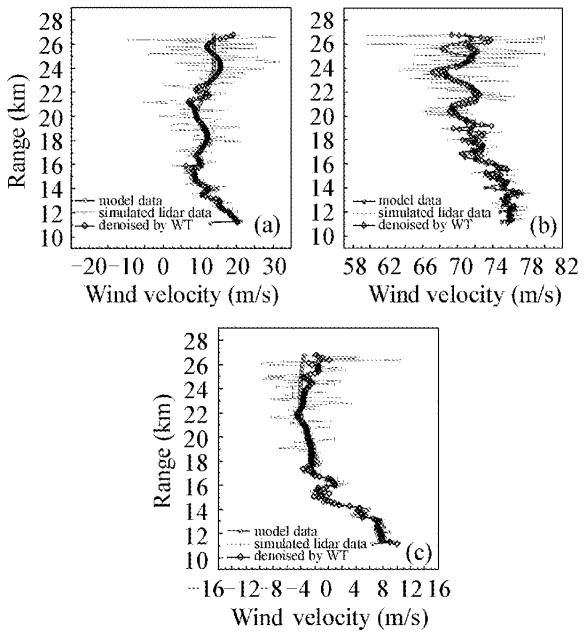

Fig. 1. LOS wind velocity profiles of true data, simulation data and denoised simulation data.

Good denoising performances at both lower altitude and higher altitude are incompatible with a single threshold. Usually, it is too noisy for higher region if the turbulences at lower region are properly reduced. On the other hand, large thresholds that are calculated in terms of the noise level at a high region will over eliminate the useful signal details, e.g. sudden change and speed vertex, at the lower region. Figures 2(f) and (g) show the denoising results with distance-dependent threshold and single threshold, respectively. The former has smaller standard deviation and correlation coefficient.

In conclusion, we have carried out an approach based on the discrete wavelet analysis of the noise reduction of Doppler lidar data. The raw wind profile contains a variety of noise and unreasonable turbulences that might obscure the actual wind information. With the proper prototype wavelet and threshold strategy, the wavelet denoising technique substantially reduces the noise and the loss of important signal information. The denoising results by comparison with *in situ* data show the potential of the wavelet denoising technique in the application of Doppler lidar.

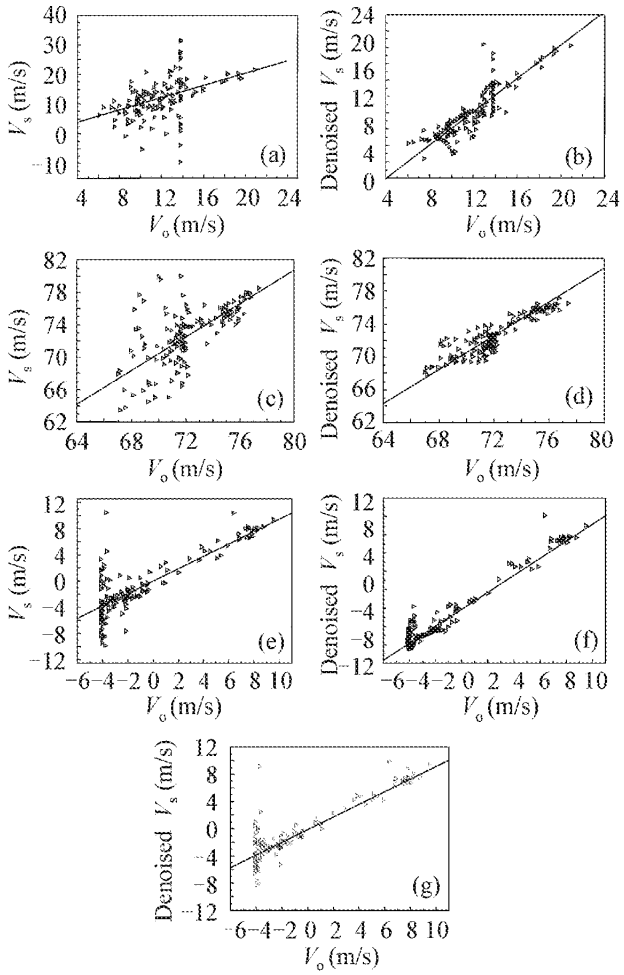

Fig. 2. Comparison between simulation wind data and wavelet denoised wind data. V: wind velocity; V_s: simulated wind velocity; V_o: original wind velocity; denoised V_s: simulated wind velocity denoised by WT. Linear regression for (a) W_1 simulation data: SD 6.15 m/s, R 0.46; (b) W_1 wavelet denoised data: SD 1.55 m/s, R 0.87; (c) W_2 simulation data: SD 3.22 m/s, R 0.59; (d) W_2 wavelet denoised data: SD 1.08 m/s, R 0.90; (e) W_3 simulation data: SD 2.62 m/s, R 0.83; (f) W_3 wavelet denoised data: SD 0.97 m/s, R 0.97; (g) W_3 wavelet denoised data using single threshold: SD 1.93 m/s, R 0.89.

This work was supported by the National High Technology Research and Development Program of China (No. 2002AA135280) and the National Natural Science Foundation of China (No. 60178017 and No. 40176011). S. Wu's e-mail address is shwu@orsi.ouc.edu.cn.

References

1. A. Gariner and M. L. Chanin, Appl. Phys. B **55,** 35 (1992).
2. C. L. Korb, B. M. Gentry, and C. Y. Weng, Appl. Opt. **31,** 4202 (1992).
3. C. L. Korb, B. M. Gentry, S. X. Li, and C. Flesia, Appl. Opt. **37,** 3097 (1998).
4. B. M. Gentry, H. Chen, and S. X. Li, Opt. Lett. **25,** 1231 (2000).
5. Z. S. Liu, W. B. Chen, T. L. Zhang, J. W. Hair, and C. Y. She, Appl. Phys. B. **64,** 561 (1997).
6. Z. S. Liu, D. Wu, J. T. Liu, K. L. Zhang, W. B. Chen, X. Q. Song, J. W. Hair, and C. Y. She, Appl. Opt. **41,** 7079 (2002).
7. Z. S. Liu, D. P. Sun, D. Wu, J. Streicher, and I. Leike, J. Ocean University of Qingdao **2,** 89 (2003).
8. I. Daubechies, IEEE Trans. Information Theory **36,** 961 (1990).
9. C. W. Kim, R. Ansari, and A. E. Cetin, in *IEEE ICASSP-92* **4,** 673 (1992).
10. D. L. Donoho, IEEE Trans. Information Theory **41,** 613 (1995).